eJSSNT Regular Paper

e-Journal of Surface Science and Nanotechnology **22**, 25–31 (2024)

Atomic and Electronic Structures on a Mordenite Zeolite

Shinya Hosokawa,[a, †] Hitoshi Sato,[b] Yasuhisa Tezuka,[c] Jun-ichi Adachi,[d] Koji Kimura,[e] Koichi Hayashi,[e] Shinji Kohara,[f] Hiroo Tajiri,[g] Kentaro Kobayashi,[a, ‡] Akihide Koura,[h] Fuyuki Shimojo [h]

[a] *Institute of Industrial Nanomaterials, Kumamoto University, Kumamoto 860-8555, Japan*
[b] *Hiroshima Synchrotron Radiation Center, Hiroshima University, Higashi-Hiroshima 739-0046, Japan*
[c] *Graduate School of Science and Technology, Hirosaki University, Hirosaki 036-8561, Japan*
[d] *Institute of Materials Structure Science (IMSS), High Energy Accelerator Research Organization (KEK), Tsukuba, Japan*
[e] *Department of Physical Science and Engineering, Nagoya Institute of Technology, Nagoya 466-8555, Japan*
[f] *National Institute for Materials Science (NIMS), Tsukuba 305-0047, Japan*
[g] *Japan Synchrotron Radiation Research Institute (JASRI), Sayo 679-5198, Japan*
[h] *Department of Physics, Kumamoto University, Kumamoto 860-8555, Japan*
[†] *Corresponding author: shhosokawa@kumamoto-u.ac.jp*
[‡] *Present address: Faculty of Materials for Energy, Shimane University, Matsue 690-8504, Japan*

Received: 1 June, 2023; Accepted: 11 August, 2023; J-STAGE Advance Publication: 21 September, 2023; Published: 21 September, 2023

Atomic structures of an insulating and hydrophobic zeolite sample of mordenite were measured by high-energy X-ray diffraction, and a pair distribution function analysis was carried out. Valence- and conduction-band O 2p partial densities of states (DOSs) in a mordenite were measured by soft X-ray emission and absorption spectroscopies (SXES and SXAS), respectively. The SXAS spectrum for the conduction band O 2p orbital has characteristic structures like that of crystalline SiO_2, while pre-shoulders are observed in mordenite. By choosing characteristic energies in the SXAS spectrum for the incident photon energies, SXES spectra were obtained, in which a large peak and three small peaks or shoulders can be assigned by a lone pair orbital and bonding (σ) ones, respectively. A density functional theory was applied to determine the exact atomic structures and electronic states, and they are in good agreement with the corresponding experiments. It is concluded that the O 2p partial DOS is mainly O-Si covalent bonds, and the Al and Na atoms have minor contributions for them. From this study, it was found that the fundamental properties of complex zeolites can only be obtained in combination of experimental and theoretical investigations as mentioned above, which can open feasibilities to uncover the origin of active sites in functional zeolites.

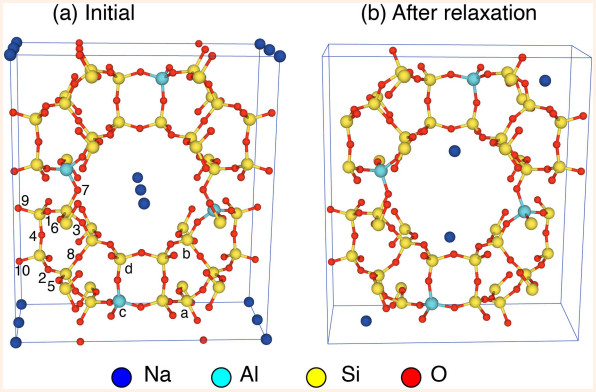

Keywords *Hydrophobic zeolite; Atomic structures; Partial electronic density of states; Density functional theory*

I. INTRODUCTION

Zeolites are functional materials that the nature manufactures by self-organizations. They are mostly composed of aluminosilicate networks with a considerable number of pores with a nanometer size in diameter [1], and only one gram of zeolite possesses a spacious surface of pores with an area wider than that of a tennis court. Zeolites have many applications, such as classical ones of molecular sieves and adsorbents for moistures, radioactive Cs ions, etc., or recently high durable exhaust gas purification devices by P-including ones, petrochemical catalysts by hydrophobic ones, antibacterial agents by Ag ions in their pores, and so on. More than two million tons of zeolites are manufactured per year all over the world, and thus, nowadays human lives do not work without zeolites.

To consider functions in zeolites, three structural parts should be carefully discussed, i.e., 1) frameworks made of mainly Si, Al, and O atoms, 2) cations located at the pore surface like Na^+ compensating the fourfold Al ions, and 3) molecules or nano-scaled atomic groups adsorbing into the pores. A variety of atomic groups can be adsorbed in the pores such as water, CO_2 [2], NO_x [3], Na [4], Se [5], Se-Te [6], etc., for which physical properties were investigated by limited experimental methods so far. Although the applications of zeolites are widely spread in human lives, basic

knowledges on these materials are not so rich, and thus, higher advancements have not been achieved on the basis of the fundamental understandings of basic scientific properties so far. This was because in addition to complex structures of zeolites, most of active sites for the functions, such as doped atoms in the frameworks, cations at the pore surfaces, and adsorbed atomic groups, have no long-range periodicity, which makes difficult to exactly determine atomic positions by usual diffraction methods. Moreover, it is difficult to measure electronic structures of zeolites by photoemission spectroscopy because they are highly insulating.

From the experimental viewpoint of atomic structures, zeolites are one of the amazing as well as complex materials because of the aforementioned combination. However, a pair distribution function (pdf) analysis becomes very effective by using high energy X-rays or neutrons from presently developed synchrotron or pulsed neutron facilities, which utilized for powder diffraction experiments on polycrystalline materials [7, 8], particularly on zeolites [9, 10]. From the experimental viewpoint of electronic structures, soft X-ray emission and absorption spectroscopy (SXES and SXAS) techniques are available for measuring the electronic density of states (DOS) of insulating materials [11]. Both involves the element and azimuthal quantum number-selective methods. In our previous reports, these methods were employed successfully to measure the O 2p partial DOS of typically insulating crystalline materials such as SiO_2 and B_2O_3 glasses [12, 13]. Moreover, theoretical calculations were performed by density functional theory (DFT) to verify the experimental data.

Mordenite ($Na_2O{\cdot}Al_2O_3{\cdot}20SiO_2$) is a typical hydrophobic zeolite. A considerable amount of mordenite is naturally produced, and thus, it is considered as one of thermally stable zeolites, and often chosen as a standard to judge the quality of other zeolites. Mordenite has one-dimensional pores with an averaged diameter of about 0.66 nm. Accordingly, it is considered as a simple zeolite among the complex material group for basic scientists, and often used for confined materials sciences such as water [14] and one-dimensional materials [5, 6]. Thus, we chose mordenite as a typical zeolite for investigating atomic and electronic structures by above-mentioned recent sophisticated experimental methods using synchrotron radiation.

In this article, we report results of high-energy X-ray diffraction (HEXRD) for investigating atomic structures, and SXAS and SXES for studying electronic structures of O 2p partial DOS. The experimental results are discussed to be reasonable by comparing with the DFT results, and the feasibility of the combination of these methods are clarified to investigate the fundamental natures of atomic and electronic structures of zeolites in general.

II. EXPERIMENTAL AND THEORETICAL PROCEDURES

Synthetic mordenite powder with a crystal size of about 1 μm was supplied by Toyo Soda Manufacturing Co., Ltd. (courtesy of Tosoh Inc.) (No. TSZ 640NAA). The mordenite powder was washed by distilled water and the powder sample was pressed to make a pellet with a diameter of 10 mm and a thickness of about 1 mm.

The HEXRD experiment was performed at BL47XU of the SPring-8, Sayo, Japan. The diffractometer installed at the beamline was originally designed for anomalous X-ray scattering experiments. To shorten the angle scanning time, the detecting system has three scintillation counters separated one another by about 30°. Each detector has an analyzer crystal of LiF with the (002) reflection to discriminate only elastic scattering signals from fluorescent and Compton scattering contributions [15] with a resolution energy of about 30 eV at the incident X-ray energy of about 25.5 keV for this experiment. The incident X-ray energy was chosen to be at 25.481 keV near the Ag Kα absorption edge, covering the wave number (Q) range up to about 190 nm^{-1}.

SXES and SXAS measurements were carried out at BL13A of the Photon Factory in the High-Energy Accelerator Research Organization (PF-KEK), Tsukuba, Japan. There, synchrotron radiation from a linear undulator device was monochromatized by a valiable-included-angle Monk-Gilliesen-type monochromator with a varied-line-spacing grating with a line density of 1000 lines mm^{-1} [16]. The SXAS spectra of O 2p conduction-band partial DOS were measured around the O K absorption edge in total electron yield mode. The energy resolution of SXAS was higher than 0.1 eV full-width at half-maximum (FWHM).

The SXES spectra were measured using a Rowland-type monochromator with a spherical grating with a radius of 5 m and a line density of 1200 lines mm^{-1} and a photon detector with a CsI-coated multichannel plate. The energy resolution of SXES was about 0.3 eV FWHM. Details of the experimental setups are given elsewhere [17]. The SXES spectra of O 2p valence-band partial DOS were obtained with incident photon energies of 535–550 eV beyond the O K absorption edge. The incident photon energies were selected at seven ones where the SXAS spectrum has characteristic structures. All the SXES and SXAS experiments were carried out at room temperature under ultrahigh vacuum condition of less than 10^{-7} Pa.

The DFT calculation was performed with a generalized gradient approximation [18] for exchange-correlation energy. Projector augmented wave potentials [19] were employed for the electron-ion interaction with the valence electron configurations of $3s^13p^03d^0$, $3s^23p^13d^0$, $3s^23p^23d^0$, and $2s^22p^4$ for the Na, Al, Si, and O elements, respectively. The electronic wavefunctions and electron density were expanded using plain wave basis sets with cutoff energies of 30 and 250 Ryd, respectively.

We used 148 atoms (4Na, 4Al, 44Si, and 96O) under a periodic boundary condition with a supercell size of 1.8131 nm × 2.0507 nm × 0.75221 nm equal to the unit cell size [20, 21]. Due to small compositions of Na and Al atoms, size effect may cause errors in the results concerning atomic and electronic structures, which should be carefully discussed. Simulations were carried out with a constant-temperature con-

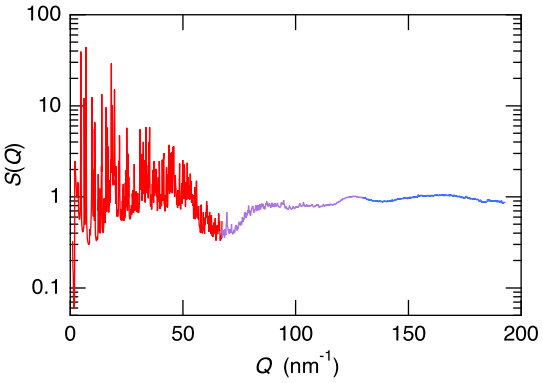

Figure 1: Logarithmic plot of $S(Q)$ spectrum on mordenite obtained from the present HEXRD experiment.

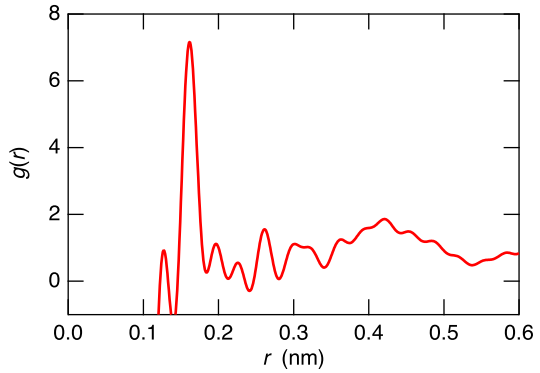

Figure 2: $g(r)$ of mordenite obtained from the present pdf analysis.

stant-volume canonical ensemble at 300 K for 8000 steps in time steps of 1.2 fs (totally 29 ps with 24000 steps). Van der Waals interactions were included using a Grimme correction [22, 23] (DFT-D method). We used our own molecular dynamics program, details of which are given in Ref. 24. The initial condition was set to be the XRD result [20, 21], and only the Na positions were set at the center of pores as explained later.

III. RESULTS

Figure 1 shows a logarithmic plot of the structure factor, $S(Q)$, of a mordenite crystal obtained by the present HEXRD experiment. The scattering data collected with three detectors are indicated by different colors in the figure. As seen in the figure, a number of Bragg peaks are observed in the diffraction pattern. The largest peak height is about 40 in the low Q range of about 5–10 nm^{-1}. The positions and heights of the Bragg peaks in the low Q region are very similar to the previous laboratory XRD works [25]. In the higher Q range beyond 70 nm^{-1}, the diffuse scattering signals dominate the $S(Q)$ spectrum. A recent theory reveals that $S(Q)$ values at the $Q \rightarrow \infty$ limit is converged to be unity owing to a multi-phonon effect even in a crystal phase [26].

Figure 2 shows the pair distribution function, $g(r)$, obtained from the present pdf analysis. As seen in the figure, the first prominent peak is observed at 0.162 nm with a height

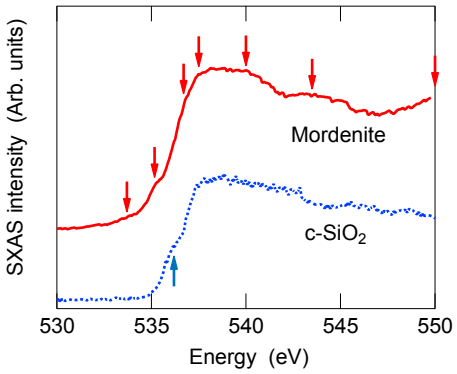

Figure 3: SXAS spectra of mordenite (solid curve) and c-SiO_2 (quartz) (dotted curve) near the O K absorption edge. For clarity, the spectra are displaced. Down arrows show the incident photon energies for the following SXES experiments. The up arrow indicates the pre-shoulder in c-SiO_2. The data of c-SiO_2 is redrawn from Ref. 12 with a permission by Physical Society of Japan.

of about 7, corresponding the first neighboring Si-O bond length of the crystal [20]. The second distinct peak is seen at 0.261 nm with a height of about 1.6, reflecting the O-O second neighboring distances in the crystal [20]. Details will be discussed later by associating with the DFT results.

The solid curve in Figure 3 shows the SXAS spectrum of mordenite near the O K absorption edge, corresponding to the O 2p conduction-band partial DOS. At a glance, the spectral feature is similar to that of single crystal (c-) SiO_2 (quartz) [12] shown as the dotted curve in the figure. In the spectrum of c-SiO_2, a pre-shoulder is observed at about 536 eV at the lower energy of the main peak at about 538 eV. These spectral features for the unoccupied O p DOS in c-SiO_2 was investigated by an electron energy-loss spectroscopy and a band structure calculation well reproduces the experimental data, where the pre-shoulder and main peak are made of O p and Si sp^3 antibonding states [27]. This is supported by the DFT calculations shown in Figure 7(a) of Ref. 12. On the other hand, the SXAS spectrum of mordenite shows several additional pre-shoulders at about 533, 535, and 537 eV. They are located at slightly different energy positions for that of c-SiO_2, and may be related to the covalent-ionic bondings of O atoms with Al and/or Na ions. Besides, there are several characteristic structures as indicated by arrows, which were used for the incident photon energies, E_0, for the subsequent SXES measurement.

The solid curves in Figure 4 shows the SXES spectra of mordenite, corresponding to the O 2p valence-band partial DOS, at several E_0 values from 533.7 to 550 eV. The SXES spectra exhibit four characteristic peaks or shoulders as indicated by dashed lines. Most of the structures do not change with varying E_0. The present SXES spectra of the mordenite sample resemble well that of a single crystal SiO_2 (quartz) sample [12] shown as the dotted curve in the figure, where the prominent peak is made of O lone-pair (LP) electrons and three structures at the lower energies correspond to the O-Si bonding (σ) states. Thus, the O 2p partial electronic structures in mordenite are dominated by O LP and O-Si σ

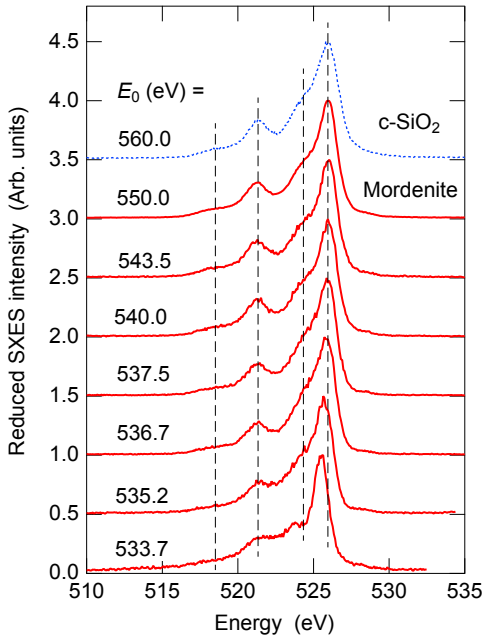

Figure 4: SXES spectra of mordenite (red solid curves), corresponding to the O 2p valence-band partial DOS, at several E_0 values from 533.7 to 550 eV, together with that of c-SiO_2 (quartz) (blue dotted curve). The energy positions of prominent structures are shown by dashed lines. For clarity, the spectra are displaced each other by 0.5. The data of c-SiO_2 is redrawn from Ref. 12 with a permission by Physical Society of Japan.

orbitals, although a small amount of Al and Na ions are contained in the mordenite sample. In combination with the SXAS spectrum in Figure 3, the band gap is estimated to be about 6 eV, smaller than that of SiO_2 crystal of about 8 eV due to the existence of the pre-shoulders at the bottom of the conduction band.

At the lower two E_0 values of 533.7 and 535.2 eV near the O K edge, however, the prominent peak at about 526 eV shifts towards the lower energies, and the shoulder at about 524 eV changes the spectral shapes. Note that these incident photon energies correspond to the energies of the pre-shoulders in the SXAS spectrum shown in Figure 3. Such spectral shifts in SXES measured at E_0 near the band gap energy were discussed on a cubic BN data by Agui *et al.* [28], who argued the relationship of this phenomenon to the indirect gap of this sample. A Raman shift [29] for SXES spectra near the bang gap energy is another possibility to explain the spectral shifts to the lower peak energies. To examine the origin of these shifts, further studies, such as electronic band calculations, are necessary, and the details cannot be discussed in this paper.

VI. DISCUSSION — COMPARISON WITH DFT CALCULATION

Figure 5 shows three-dimensional atomic configurations obtained (a) before and (b) after the structural relaxation by the DFT calculation. Bonds are indicated when the inter-

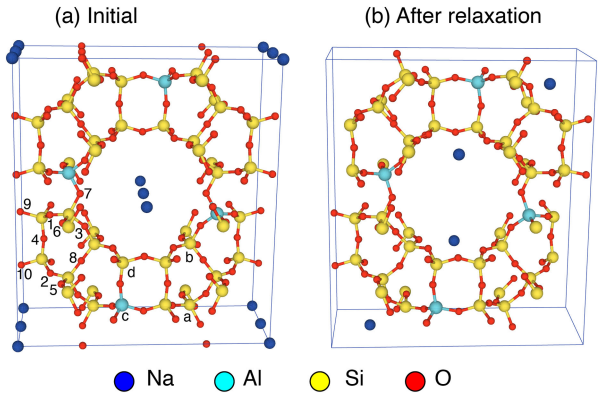

Figure 5: Three-dimensional atomic configurations (a) before and (b) after the DFT relaxation. The numbers and alphabets in (a) indicate ten and four different sites for the O and Si/Al atoms, respectively.

atomic distance is less than 0.20 nm. Here, we explain the atomic configurations of mordenite in detail by using initial configurations [20, 21] shown in Figure 5(a). The Si and Al atoms are fourfold coordinated with the twofold coordinated O atoms to form the zeolite frame. The O atoms have 10 different crystallographic sites as shown by the numbers in Figure 5(a). The Si/Al atoms have 4 different sites as given by the alphabets in the figure. Two Al atoms out of four are located at the 'a' site and the other two at the 'c' sites as seen in Figure 5(a) so that the Al atoms have long distances of about 1 nm between them. Four Na atoms stand at the center of 12-membered rings of the pores, in which two are at the central pore and other two are in another pore in Figure 5(a).

The aluminosilicate framework changes very slightly by the DFT relaxation, whereas the positions of two Na atoms in the pore center largely move to the surface of the pores having short interatomic distances with O atoms as shown in Figure 5(b). We performed the calculations for several times by changing the initial atomic configurations along the pore directions in Figure 5(a), and the resultant Na positions are at mostly the same pockets on the pore surface as shown in Figure 5(b). This would be because the calculation temperature of 300 K is high and the Na atoms have enough free volume for the movements around them in the pores. Note that the Na atoms seem to locate apart from the Al atoms, which contradicts the preliminary idea of the charge distributions in zeolites, i.e., Na^+ and Al^- [30]. Since diffraction methods can determine only the average positions in the lattice, and their results do not guarantee the real atomic positions [31]. Therefore, the obtained result from the DFT relaxation is reasonable.

Figure 6(a) shows total X-ray pair distribution functions, $g(r)$, obtained by the present DFT calculation, multiplied by the averaged weighting factors of X-ray scattering to compare with the experimental XRD data shown by the thin solid curve. The plenary peak is located at 0.164 nm, which is in good agreement with the experimental result at 0.162 nm, although the peak height is much higher. The second peak appears at 0.268 nm, which is again in good agreement with

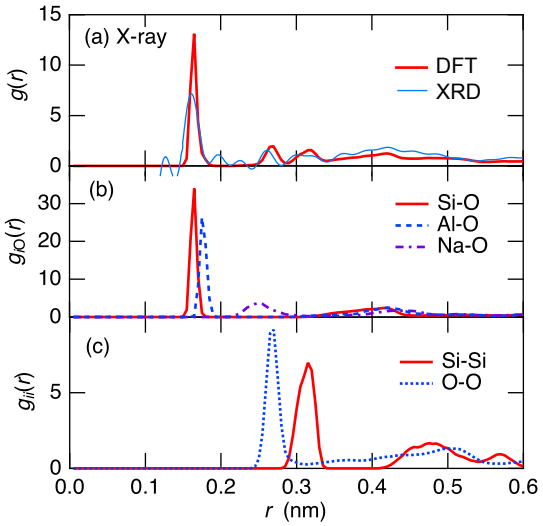

Figure 6: (a) $g(r)$, (b) $g_{iO}(r)$, and (c) $g_{ii}(r)$ functions obtained from the present DFT calculation. The thin solid curve in (a) shows the result of HEXRD experiment (the same as in Figure 2) for the comparison.

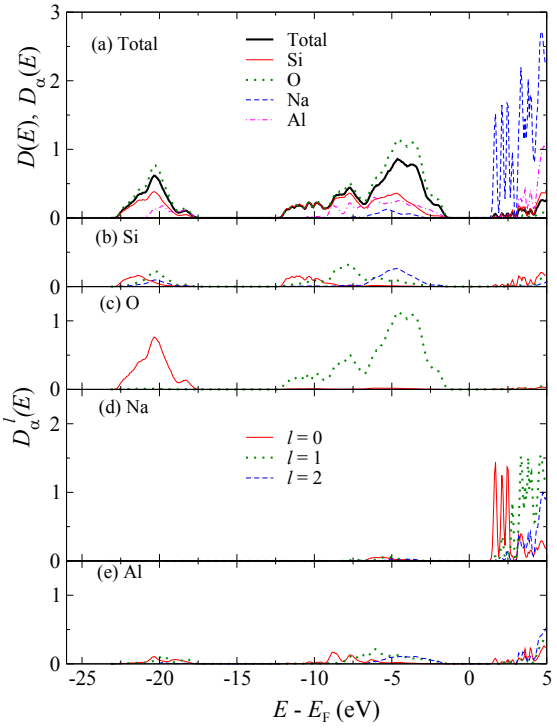

Figure 7: DFT results for (a) total DOS, $D(E)$, and the elementally partial ones, $D_\alpha(E)$, and the orbital angular momentum contributions, $D^l_\alpha(E)$, of (b) Si, (c) O, (d) Na, and (e) Al.

the experiment at 0.261 nm. Relatively broad and asymmetric third and fourth peaks are observed at about 0.32 and 0.42 nm, respectively. These peaks are also observed experimentally in Figure 2.

To clarify the element-selective information about these structures in $g(r)$, selected partial pair distribution functions, $g_{ij}(r)$, are given in Figure 6(b, c). In (b), the correlations with O are summarized as solid, dashed, and chain curves for Si-O, Al-O, and Na-O, respectively. As clearly seen in the figure, the prominent peak for $g(r)$ is mostly composed of the Si-O partial with the position of 0.164 nm. In addition, the main part of the fourth broad and asymmetric peak at about 0.42 nm seems to be made of the Si-O correlation. The Al-O bond length is determined to be 0.176 nm, which was also obtain in the Na 4A type zeolite [10]. Owing to a small composition of Al, i.e., Al/Si = 1/11 in the DFT calculation, however, the Al-O peak cannot be visualized in Figure 6(a). On the other hand, the Na-O interatomic distance is found to be 0.250 nm, indicating that the Na atoms are not located in the frame of the zeolite. Due to the low concentration of Na atoms, this peak is not clearly observed in Figure 6(a).

Figure 6(c) shows the Si-Si (solid curve) and O-O (dotted curve) partials. The O-O interatomic distance is given to be 0.268 nm, corresponding to the second peak in $g(r)$ at the same position. This peak corresponds to the O-O distance in the SiO_4 tetrahedra, and mostly coincides with the experimental peak position of 0.261 nm shown in Figure 2. The Si-Si correlation appears as an asymmetric peak at the top position of 0.314 nm. This Si-Si interatomic distance corresponds to that between the SiO_4 tetrahedra, and the distribution is reflected by a variety of the Si-O-Si bond angles in the crystal [20, 21] as shown in Figure 5. The other five $g_{ij}(r)$ functions are negligible in the total $g(r)$ owing to the small compositional fractions of Al and Na.

Figure 7 shows the theoretical result for (a) total DOS, $D(E)$, the elementally partial ones, $D_\alpha(E)$, and the orbital angular momentum contributions, $D^l_\alpha(E)$, of (b) Si, (c) O, (d) Na, and (e) Al obtained by the DFT calculation as a function of energies with respect to the Fermi energy, E_F. Here, E_F is defined approximately at the center of the band gap in $D(E)$. The $D(E)$ function shown in (a) by the black solid curve is separated into $D_\alpha(E)$s given by colored curves. The $D_\alpha(E)$s are divided into $D^l_\alpha(E)$s with orbital angular momentum numbers l, such as s, p, and d electrons corresponding to $l = 0$, 1, and 2, respectively. The present experimental SXAS and SXES data should correspond to $l = 1$ in (c) O partials (the dotted curve). The band gap energy obtained from the present DFT calculation is about 4 eV, smaller than the experimental value. It is well-known that DFT calculations usually underestimate the magnitude of band gap [32], in particular oxide materials.

The present theoretical result of the O 2p valence-band DOS in the shallow energy range between −2 and −13 eV is in good agreement with the present SXES data, which shows the distinct LP band at about −4 eV and three σ states between −5 and −12 eV at the proper energy positions. The hybridizations of the O 2p states mostly take place with the Si 3s and 3p electrons depending on the (binding) energy, E, which is a typical feature of the sp^3 hybridization of Si in SiO_2 [12, 33]. The contributions of the Na and Al atoms are very small, because the spectra in Figure 7(d, e) are small and the compositions of these elements are also small. Note that the vertical axis in this figure is shown DOSs per one atom.

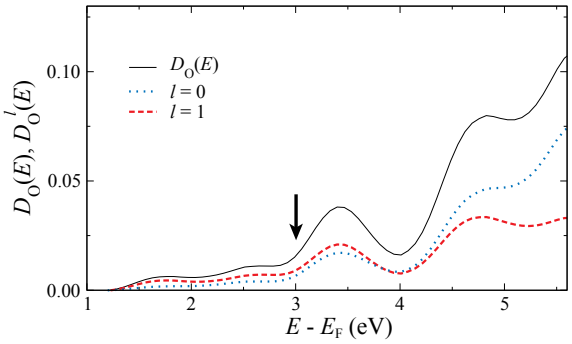

Figure 8: The enlarged spectra of the O contributions in the conduction band range. The solid, dotted, and dashed curves represent the total, s, and p partial O spectra, respectively.

Concerning the conduction-band DOS, the calculated O 2p partial DOS is very small. On the other hand, the Si 3s and 3p states largely contribute the main part of the conduction band at energies beyond about 3 eV. This feature is reasonable when assuming the typical feature that the conduction band is composed of Si-O anti-bonding state and the fraction of Si sp^3 states is much larger than the O 2p state in the conduction band region [33, 34].

The SXAS spectra basically originate from only the O 1s-2p excitations, and thus, it is necessary to observe the theoretical O 2p contributions. Figure 8 shows the enlarged spectrum of the O contribution, $D_O(E)$, in the conduction band range. The red dashed curve shows the corresponding O p electron DOS. The main conduction band edge is approximately located at 3 eV as indicated by the arrow, corresponding the experimental SXAS data at about 535.5 eV in Figure 3. The structural features basically coincide with the experimental SXAS data although the 4 eV dip is buried probably because of the inaccuracies of the DFT calculation and the insufficient energy resolution of experiment. Concerning the pre-shoulders, there are two small and broad peaks between 1.5–3.0 eV above E_F as seen in the figure, which proves the existence of the pre-shoulders in the experimental SXAS data in Figure 3. As seen in Figure 7(d), the Na 3s electrons contribute the pre-shoulders, while the Si 4s electrons may also intervene there because the Si composition is large. The O 1s-2p SXAS spectrum does not originate only from the simple 1s-2p direct optical transition, but it would be necessary to consider the effect of the core hole in the final state, which may also the reason why the coincidence of the experimental and theoretical results on the conduction band are not enough satisfactory. Thus, we judged at present that the discussion about the comparison between the results of the SXAS experiment and DFT calculation is difficult to proceed further.

V. CONCLUSION AND PERSPECTIVE

In this paper, we present atomic structures by HEXRD with the pdf analysis, O 2p partial electronic DOSs on an insulating mordenite sample obtained by SXAS and SXES experiments, and a DFT calculation. The atomic structures are in excellent agreement with the present DFT results. The SAXS spectrum for the O 2p conduction band is very similar to that of SiO_2 crystal, indicating that the O 2p partial electronic states in the mordenite is composed of mostly O-Si interactions. The SXES spectra for the O 2p valence band have characteristic structures of LP and σ orbitals, which resemble well those of SiO_2 crystal. According to the present results, we concluded that the experimental and theoretical methods used in the present studies are very feasible and promising to investigate the fundamental properties of atomic and electronic structures on structurally complex zeolite materials.

Here, we mention our future plan how to solve the present discrepancies between the experiment and the DFT calculation, As pointed out above, the calculation size was only one unit cell, and only four Na and Al atoms were included in the present calculation, which may induce the disagreements with the experimental data of the electronic structures. Therefore, a larger calculation box of at least four unit cell containing about 600 atoms or more preferably 32 unit cells with about 5000 atoms would be required, whereas a typical computational power in the laboratory forbids such calculations with such large scales. To overcome the computational limitations, an algorithm of artificial neural network (ANN) potential was proposed by Behler and Parrinello [35], which creates an ANN empirical potential by training an empirical potential with a limited DFT result using a super computer. By using this method, the calculation could be conducted with a first-principles accuracy but over 10^4 times shorter computing time [36], which is helpful to confirm the present knowledge on the structurally complex zeolites.

The aim of this paper is to study the fundamental properties of atomic and electronic structures of mordenite as a reference for studying further complex zeolites with functional properties. For the applicational uses of zeolites, substitutional exchanges of functional elements are made in either zeolite frames, compensated cations, or pore holes. The examples of the applications are described in the first paragraph of the Introduction section, and the substitution of Sn atoms into mordenite is highly related to the CO_2 absorption. For the first stage of these subsequent studies, it is important to obtain information about a reference zeolite without dopant elements for the further investigations to find a role of dopant element as an active site. Our first trial was very recently published on a Ag-containing 4A type zeolite having an antibacterial function [10].

Acknowledgment

The HEXRD experiment was carried out at BL47XU of the SPring-8 (No. 2023A1346). The SXAS and SXES experiments were performed at BL13A in the PF-KEK (Nos. 2018G597 and 2020G541). This work was supported by JSPS Grant-in-Aid for Transformative Research Areas (A) 'Hyper-Ordered Structures Science' (No. 21H05569 for SH and KKo, 23H04117 for SH, and 20H05881 for KKi, KH, SK, and HT) and for Scientific Research

(C) (No. 22K12662 for SH), and the Japan Science and Technology Agency (JST) CREST (Nos. JPMJCR1861 for SH and KKo and JPMJCR18I2 for AK and FS).

References

[1] D. W. Breck, *Zeolite Molecular Sieves: Structure, Chemistry, and Use* (Wiley, New York, 1974).
[2] D. Bonenfant, M. Kharoune, P. Niquette, M. Mimeault, and R. Hausler, Sci. Technol. Adv. Mater. **9**, 013007 (2008).
[3] M. Colombo, I. Nova, and E. Tronconi, Catal. Today **151**, 223 (2010).
[4] T. Ikeda, T. Nakano, and Y. Nozue, J. Phys. Chem. C **118**, 23202 (2014).
[5] K. Tamura, S. Hosokawa, H. Endo, S. Yamasaki, and H. Oyanagi, J. Phys. Soc. Jpn. **55**, 528 (1986).
[6] M. Inui, M. Yao, and H. Endo, J. Phys. Soc. Jpn. **57**, 553 (1988).
[7] V. Petkov, I.-K. Jeong, J. S. Chung, M. F. Thorpe, S. Kycia, and S. J. L. Billinge, Phys. Rev. Lett. **83**, 4089 (1999).
[8] T. Egami and S. J. L. Billinge, *Underneath the Bragg Peaks: Structural Analysis of Complex Materials* (Pergamon, Amsterdam, 2003).
[9] M. M. Martínez-Iñesta, I. Peral, T. Proffen, and R. F. Lobo, Stud. Surf. Sci. Catal. **154**, 1393 (2004).
[10] S. Hosokawa, K. Kobayashi, A. Koura, F. Shimojo, Y. Tezuka, J. Adachi, Y. Onodera, S. Kohara, H. Tajiri, A. Chokkalingam, and T. Wakihara, Microporous Mesoporous Mater. **359**, 112662 (2023).
[11] A. Kotani and S. Shin, Rev. Mod. Phys. **73**, 203 (2001).
[12] S. Hosokawa, H. Sato, K. Mimura, Y. Tezuka, D. Fukunaga, Y. Matsuzaki, and F. Shimojo, J. Phys. Soc. Jpn. **84**, 024605 (2015).
[13] S. Hosokawa, H. Sato, K. Mimura, Y. Tezuka, D. Fukunaga, K. Shimamura, and F. Shimojo, J. Phys. Soc. Jpn. **83**, 114601 (2014).
[14] V. Dondur and R. Dimitrijevic, Stud. Surf. Sci. Catal. **24**, 345 (1985).
[15] S. Kohara, H. Tajiri, C. H. Song, K. Ohara, L. Temleitner, K. Sugimito, A. Fujiwara, L. Pusztai, T. Usuki, S. Hosokawa, Y. Benino, N. Kitamura, and K. Fukumi, J. Phys. Conf. Ser. **502**, 012014 (2014).
[16] A. Toyoshima, T. Kikuchi, H. Tanaka, K. Mase, K. Amemiya, and K. Ozawa, J. Phys. Conf. Ser. **425**, 152019 (2013).
[17] S. Shin, A. Agui, M. Fujisawa, Y. Tezuka, T. Ishii, and N. Hirai, Rev. Sci. Instrum. **66**, 1584 (1995).
[18] J. P. Perdew, K. Burke, and M. Ernzerhof, Phys. Rev. Lett. **77**, 3865 (1996).
[19] P. E. Blöchl, Phys. Rev. B **50**, 17953 (1994).
[20] P. Simoncic and T. Armbruster, Am. Mineral. **89**, 421 (2004).
[21] K. Shiokawa, M. Ito, and K. Itabashi, Zeolites **9**, 170 (1989).
[22] S. Grimme, J. Antony, S. Ehrlich, and H. Krieg, J. Chem. Phys. **132**, 154104 (2010).
[23] S. Grimme, S. Ehrlich, and L. Goerigk, J. Comput. Chem. **32**, 1456 (2011).
[24] F. Shimojo, S. Fukushima, H. Kumazoe, M. Misawa, S. Ohmura, P. Rajak, K. Shimamura, L. B. Oftelie, S. Tiwari, R. K. Kalia, A. Nakano, and P. Vashishta, SoftwareX **10**, 100307 (2019).
[25] V. Gramlich, *Untersuchung und Verfeinerung Pseudosymmetrischer Strukturen*, Ph.D. thesis, ETH, Zurich, 1971: M. M. J. Treacy and J. B. Higgins (Eds.), *Collection of Simulated XRD Powder Patterns for Zeolites* (Elsevier, Amsterdam, 2001), pp. 244-245.
[26] H. Kitamura, Acta Crystallogr. A **78**, 415 (2022).
[27] L. A. J. Garvie, P. Rez, J. R. Alvarez, P. R. Buseck, A. J. Craven, and R. Brydson, Am. Mineral. **85**, 732 (2000).
[28] A. Agui, S. Shin, M. Fujisawa, Y. Tezuka, T. Ishii, Y. Muramatsu, O. Mishima, and K. Era, Phys. Rev. B **55**, 2073 (1997).
[29] H. Ishii, Y. Ishiwata, R. Eguchi, Y. Harada, M. Watanabe, A. Chainani, and S. Shin, J. Phys. Soc. Jpn. **70**, 1813 (2001).
[30] J. Sauer, Chem. Rev. **89**, 199 (1989).
[31] For example, S. Hosokawa, N. Happo, S. Senba, T. Ozaki, T. Matsushita, A. Koura, F. Shimojo, and K. Hayashi, J. Phys. Soc. Jpn. **83**, 124602 (2014).
[32] K. A. Johnson and N. W. Ashcroft, Phys. Rev. B **58**, 15548 (1998).
[33] J. R. Chelikowsky and M. Schlüter, Phys. Rev. B **15**, 4020 (1977).
[34] Z. Y. Wu, F. Jollet, and F. Seifert, J. Phys. Condens. Matter **10**, 8083 (1998).
[35] J. Behler and M. Parrinello, Phys. Rev. Lett. **98**, 146401 (2007).
[36] K. Shimamura, S. Fukushima, A. Koura, F. Shimojo, M. Misawa, R. K. Kalia, A. Nakano, P. Vashishta, T. Matsubara, and S. Tanaka, J. Chem. Phys. **151**, 124303 (2019).